

## Studies of wall temperature effects on shock-wave/boundary layer interactions in hypersonic flow

by A.Ciani, S.Paris, D.G.Fletcher

*von Karman Institute for Fluid Dynamics, Aerodynamic and Aerospace Department.  
72, Chaussée de Waterloo - Rhode Saint-Genèse - Belgium*

### Abstract

Infrared thermography equipment is used to measure the temperature rise at a surface of a model simulating a deflected flap of a re-entry vehicle. The model is tested in the VKI-H3 hypersonic wind tunnel with a flow at Mach 6 at different Reynolds numbers and temperatures. Examining the rise of temperature on the interested surface, it is possible to visualize the flow topology on the surface and to infer the heat flux on the model. By heating artificially the model before the tests it is possible to evaluate the effects of the wall temperature on heat flux and flow topology.

### Nomenclature

Cp:	specific heat for air at constant pressure [ $\text{J kg}^{-1} \text{K}^{-1}$ ]	t:	time [s]
k:	thermal conductivity [ $\text{W m}^{-1} \text{K}^{-1}$ ]	T:	temperature [K]
h:	convective heat transfer coefficient [ $\text{W m}^{-2} \text{K}^{-1}$ ]	x,y,z:	Cartesian co-ordinates [m]
H:	total enthalpy [ $\text{J kg}^{-1}$ ]	$\alpha$ :	thermal diffusivity [ $\text{m}^2 \text{s}^{-1}$ ]
M:	Mach number [-]	$\gamma$ :	ratio of specific heats [-]
P:	pressure [Pa]	$\rho$ :	density [ $\text{kg m}^{-3}$ ]
$\dot{q}$ :	heat flux [ $\text{W m}^{-2}$ ]	$\infty$ :	infinity condition
r:	recovery factor [-]	aw:	adiabatic wall
Ch:	Stanton number [-]	w:	wall condition
		o:	total or stagnation condition
		e:	edge condition

### 1. Introduction

The development of hypersonic vehicles has brought renewed attention to the problem of viscous-inviscid flow interaction phenomena that are of great practical importance for wing/body junctures and deflected control surfaces. Prediction of thermal loads on surfaces exposed to hypersonic flow is an essential prerequisite for the effective design of aerodynamic control surfaces and thermal protection systems (TPS) of proposed space vehicles that will enable trans-atmospheric flight. In this context, the interaction of shock waves with boundary layers on surfaces at relatively high temperature is an important aspect of hypersonic fluid dynamics because of their frequent occurrence in applications and subsequent impact on the behavior of the boundary layer. In particular the extension of the resulting separation bubble is of prime importance because pressure and heat transfer reach a maximum in the reattachment region.

Wall temperature can have an effect on the size of the separated zone and separation point, pressure level and heat transfer. This is why it is necessary to investigate the phenomena at different wall temperatures.

### 2. Theoretical approach

Flows are considered to be hypersonic when the local Mach number, M is greater than 5 [1]. Hypersonic flows are characterized by the presence of real gas effects (wall

temperature heating because of high recovery temperature, ionization, dissociation), which become progressively more important as the Mach number is increased.

A control surface of a hypersonic vehicle can be simulated with a ramp as shown in figure 1. Within the boundary layer in the first part of the model (flat plate), it is possible to find a subsonic region. Thus the adverse pressure gradient caused by the compression corner can be felt upstream and thereby cause a separation of the flow. Upstream of the separation it is possible to see the thickness of the boundary layer increasing and a series of compression waves (Mach lines) that merge into a shock wave. As shown in figure 1, a recirculation bubble appears, followed by a reattachment point with another shock wave.

The viscous interaction in a hypersonic flow causes large energy transfer from the flow to the model. It is possible to measure the wall temperature evolution with the infrared camera, which allows a determination of the wall heat flux by using a transient conduction analysis.

We make use of the semi-infinite slab model hypothesis:

The model is semi-infinite in thickness; heat conduction into this slab is one-dimensional. This hypothesis is not valid in the neighborhood of the edges where large lateral temperature gradients are found and lateral conduction becomes an important factor.

The thermal properties of the slab are uniform and do not depend on temperature.

For the model used in this project an insulator (Vespel®) with a thickness of 5mm was used. It was calculated that this layer can be compared with a layer of infinite thickness for the time (2 seconds) during which a test takes place.

The equation to solve is:

$$\frac{\partial^2 T}{\partial x^2} + \frac{\partial^2 T}{\partial y^2} + \frac{\partial^2 T}{\partial z^2} - \frac{1}{\alpha} \frac{\partial T}{\partial t} = 0 \quad (1)$$

with

$$\alpha = \frac{k}{\rho C_p} \quad (2)$$

For the one-dimensional case this becomes:

$$\frac{\partial^2 T}{\partial x^2} = \frac{1}{\alpha} \frac{\partial T}{\partial t} \quad (3)$$

The heat transfer at the wall is evaluated by the use of a dimensionless parameter: the Stanton number, defined as:

$$Ch = \frac{\dot{q}}{\rho_\infty U_\infty C_p (T_r - T_w)} \quad (4)$$

where  $T_r$  is the recovery temperature. The recovery temperature is a hypothetical temperature for which there is no convective exchange between the flow and the surface [1]. It is defined by:

$$T_r = T_e \left( 1 + r \frac{\gamma - 1}{2} M_e^2 \right) \quad (5)$$

the recovery factor  $r$  is defined as  $r = (H_{aw} - H_e) / (H_0 - H_e)$ .

For the data reduction the hypothesis of constant convective heat transfer coefficient  $h$  was assumed. This assumption is possible because the images to be processed are only 30, taken in two seconds. During this period there is the change in temperature shown in figure 3 that never exceeds  $10^{\circ}\text{C}$ . This temperature change cannot affect the heat transfer coefficient more than 3%.

### 3. Experimental approach

A new model was designed and constructed to simulate the deflected flap of a re-entry vehicle. A heating system for the model was also fabricated and a regulation system was implemented to maintain the temperature of the model at a preset value. Tests were made with the model in the VKI-H3 facility and infrared images were recorded with the Agema 900 IR camera.

The VKI hypersonic tunnel H3 is a blowdown facility with an axisymmetric nozzle. The nozzle, which has an exit diameter of 15 cm, produces a nearly uniform Mach 6 free jet flow of 12 cm in diameter. To avoid condensation of the air, which is initially stored at ambient temperature in the high pressure reservoirs, it is heated in a storage heat exchanger before entering the tunnel's settling chamber. To achieve the high pressure ratio between the tunnel settling chamber and the exit of the diffuser, a supersonic ejector is used to provide the necessary suction at the downstream end of the diffuser. A mechanism for rapid injection of models is available. To prevent blockage in the tunnel and to avoid non uniform heating of the model, the model is kept outside of the flow during the start-up of the facility. Once the flow is established the model is injected into the free jet (injection by a pneumatic system within 0.25 second). The total pressure of the test is controlled by the operator, and typically, experiments are done at 3 different pressures: 11, 21 and 31 bars (corresponding to Reynolds numbers: 8,16 and 23  $10^6[1/m]$ ). During the short duration test, constant reservoir conditions may be maintained. A measure of total pressure and temperature in the settling chamber is made to record the test conditions for each run. To enable temperature measurements by using infrared thermography, the test section is equipped with a germanium window of 80 mm diameter placed at the lateral part of the tunnel test chamber at a distance of 0.6 m from the flow.

The infrared camera is the AGEMA LW 900 which measures radiation in the wavelength range between 8 and 12  $\mu\text{m}$ . Images are obtained from a system of a rotating prism and oscillating mirror. The acquisition frequency is 15 Hz. The output is not given as a temperature, but an intensity proportional to the radiant flux emanating from the target. This intensity of heat flux can be converted to temperature values by calibration. The relation between intensity and temperature is described by the equation

$$T[^{\circ}\text{C}] = -5.38 \cdot 10^{-5} \cdot I^2 + 0.2052 \cdot I - 64.64$$

This calibration is done with the model painted in black inside the wind tunnel thereby including the germanium window absorption.

The model has a ramp with a  $10^{\circ}$  deflection angle as shown in figure 2. Heating elements were placed inside the model, to distribute the heat by conduction using an aluminum (high conductive material:  $k_{al}=200 \text{ WK}^{-1}\text{m}^{-1}$ ) frame. To facilitate the measurements and to simulate a semi-infinite slab, an insulated surface was used. A layer of 'Vespel®' was used on the surface of the model to provide this insulating material. Vespel® is a polymer that can withstand high temperatures, yet is relatively easy to machine. A blunt leading edge was chosen with a radius of 0.5mm. Tight tolerances were specified on the interfaces between the aluminum part and the Vespel® to avoid steps and gaps between them; in particular near the leading edge. The layer in Vespel® was fixed by three particular screws to allow small relative movements between aluminum and Vespel® due to differential thermal expansion while maintaining alignment of critical features. Because of heat losses from the surface of the model, a temperature gradient was expected to be found inside the Vespel® layer. To avoid this, a plate in aluminum was constructed and equipped with another independent heating system. When heated to the same temperature

of the model and placed in front of it, the plate can reduce heat losses to a minimum because the temperature difference between the model and the plate is negligible. Once the desired Vespel® surface temperature was reached, the following steps were taken: Start recording total pressure and temperature on a pen-plotter; evacuate the tunnel; inject the model in the test section; record the reference image (for initial temperature); remove the model; open the fast acting valve and wait for the flow in the test section to be established; start to record a sequence and inject the model; after recording at least 30 images (2 seconds) stop recording; retract the model and stop the wind tunnel.

#### 4. Analysis and results

For every test a sequence of images was recorded. This series of images was stored by the IR camera in one file. Every sequence was modified so to have, as the first image, the reference image without flow and, from the second image on, the thermograms acquired with the model completely injected in the flow. This is a procedure that has to be done manually using the Agema900 system to remove all the images obtained during the insertion of the model into the flow (where flow conditions were not steady). The sequences were then processed to evaluate the Stanton number distribution on each part of the model. However, only measurements made on the Vespel® surface (insulating) were in agreement with the assumption of a semi-infinite slab, thus it was necessary to define exactly on which image pixels data processing was to be done. For this purpose, some images were extracted from the test sequences in tecplot format to decide on which part the Stanton number evaluation would be performed. From the images it was possible to visualize the different temperatures on the model and thus have an idea of the flow topology and the quality of the measurement. It was best to make computation always on the central line of the model to avoid lateral effects on the measurements. It is possible to observe in figure 3 a graph showing the temperature distribution on the centerline of the model during a test at 300K surface temperature and 21bar total pressure. The large gap between the first and second temperature distributions is due to the 'non information' during the injection process. In fact the first image ( $t_1=0\text{sec}$ ) is the reference image and the following one is the first image after injection.

The Stanton number distribution was always calculated on the central line of the model from the leading edge but only on the part in Vespel®. A typical distribution is shown in figure 4 for three different Reynolds numbers (pressures). For these tests the wall temperature was ambient temperature (300K). From this plot it is possible to identify the position of the recirculation bubble, and the separation and reattachment points. In figure 4 for all three conditions the separation and reattachment points are at the same place, i.e. they are independent of the flow Reynolds number. To locate these points it was assumed that the recirculation bubble starts and ends at the point where the slope of the Stanton number curve changes more (i.e. the maximum of the second derivative). The flow topology varies with Reynolds number, in fact the complete laminar case of 11bar becomes transitional for 21bar (sharp increase of the Stanton number) and turbulent for the 31bar case.

In figure 5, tests at higher wall temperature (400K) are presented. For the hot wall case there is not an evident change in Stanton number along the model. That could be explained by the destabilizing effect of increased wall temperature [2]. It is possible that the flow is turbulent along all the model. This hypothesis was validated by performing experiments at high total pressure conditions with a perturbation near the leading edge to be sure that the flow was turbulent. The perturbation was a 0.5 mm step glued on the surface at 2cm from the leading edge. It was found that the Stanton number distribution remains very similar to that one shown in figure 5.

Measurements were also performed at 500K, but the computed heat flux was comparable to the noise of the measurements since the wall temperature was very close to the stagnation temperature.

## 5. Conclusion

Experimental investigations were carried out on a model simulating a control surface (such as an open flap of a wing) in a hypersonic flow. The model geometry was a 2D ramp and this model was tested in the VKI-H3 hypersonic wind tunnel in a Mach 6 flow. Infrared thermography was the main measurement technique. To produce more realistic simulation of actual flight conditions in the facility, the model was designed to allow an investigation of the effects of  $T_w/T_r$  parameter. The model was heated to three different temperatures, namely 300K, 400K and 500K. Tests were done at three different Reynolds numbers, corresponding to 11bar, 21bar and 31bar total pressure in the H3 facility. With this model it was possible to simulate hot-wall conditions with  $T_w/T_r=0.66$  for the tests without heating,  $T_w/T_r=0.88$  for test at medium temperature and  $T_w/T_r>1$  for the hottest cases where it is possible to see negative heat flux.

The flow topology was studied and quantitative measurements of the heat flux were obtained for the different conditions. It was possible to locate the flow separation and reattachment points, and these findings were compared with skin friction measurements performed on the same model using 'oil-film interferometry' and a discrepancy of only few millimeters was found for the location of separation and reattachment points. The Stanton number distribution is calculated and compared between the different cases. Laminar, transitional and turbulent conditions are observed. A destabilizing effect is caused by increasing wall temperature.

## References

- [1] J.D.ANDERSON, "Hypersonic and High Temperature Gas Dynamics", McGraw Hill, 1989.
- [2] A.H.SHAPIRO, "The Dynamics and Thermodynamics of Compressible Fluid Flow", The Ronald Press Company, New York, 1954.

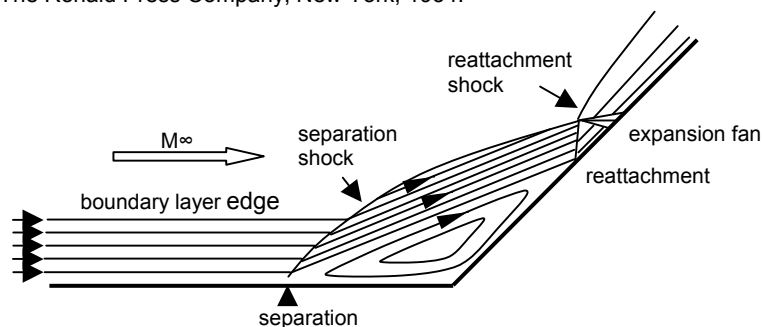


Fig. 1. Model simulating a control surface.

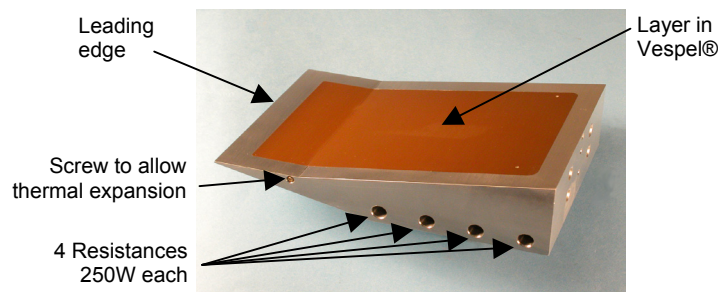


Fig. 2. Model used for tests in H3

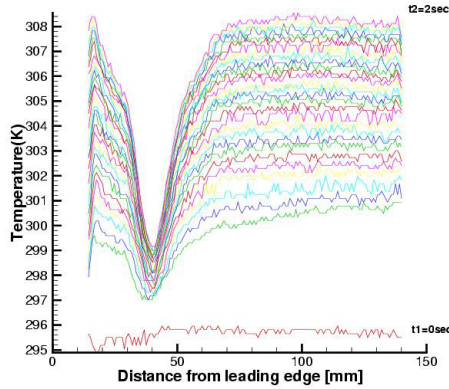


Fig. 3. Temperature rise during a test with  $T_w=300K$   $P_0=21bar$

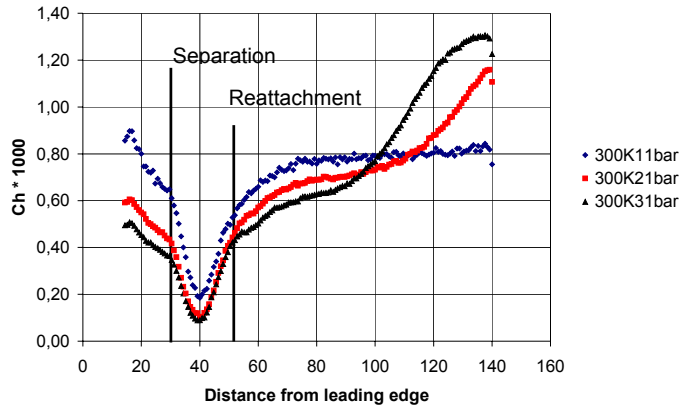


Fig. 4. Stanton number distribution on the centerline for three different Reynolds numbers - cold tests.

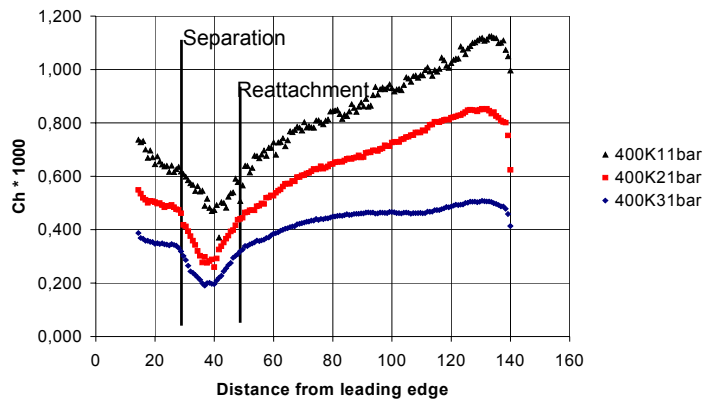


Fig. 5. Stanton number distribution on the centerline for three different Reynolds numbers - hot tests.